HHS Public Access

Author manuscript

J Comp Neurol. Author manuscript; available in PMC 2015 December 28.

Published in final edited form as:

J Comp Neurol. 2014 April 15; 522(6): 1232–1248. doi:10.1002/cne.23465.

Differences in Spinal V2a Neuron Morphology Reflect Their Recruitment Order During Swimming in Larval Zebrafish

Evdokia Menelaou[1], **Cassandra VanDunk**[1], and **David L. McLean**[1,*]

[1] Department of Neurobiology, Northwestern University, Evanston, Illinois 60208, USA

Abstract

Networks of neurons in spinal cord generate locomotion. However, little is known about potential differences in network architecture that underlie the production of varying speeds of movement. In larval zebrafish, as swimming speed increases, Chx10-positive V2a excitatory premotor interneurons are activated from ventral to dorsal in a topographic pattern that parallels axial motoneuron recruitment. Here, we examined if differences in the morphology and synaptic output of V2a neurons reflect their recruitment order during swimming. To do so, we used *in vivo* single cell labeling approaches to quantify the dorso-ventral distribution of V2a axonal projections and synapses. Two different classes of V2a neurons are described; cells with ascending and descending axons, and cells that are only descending. Among the purely descending V2a cells, more dorsal cells project longer distances than ventral ones. Proximally, all V2a neurons have axonal distributions that suggest potential connections to cells at and below their own soma positions. At more distal locations, V2a axons project dorsally, which creates a cumulative intersegmental bias to dorsally located spinal neurons. Assessments of the synapse distribution of V2a cells, reported by synaptophysin expression, support the morphological observations and also demonstrate that dorsal V2a cells have higher synapse densities proximally. Our results suggest that V2a cells with more potential output to spinal neurons are systematically engaged during increases in swimming frequency. The findings help explain patterns of axial motoneuron recruitment and set up clear predictions for future physiological studies examining the nature of spinal excitatory network connectivity as it relates to movement intensity.

Graphical Abstract

* Contact: david-mclean@northwestern.edu; TEL: +1 847 467 1696; FAX: +1 847 491 5211.

Author contributions

All authors had full access to all the data in the study and take responsibility for the integrity of the data and the accuracy of the data analysis. Study concept and design: E.M., C.V., D.M. Acquisition of data: E.M., C.V. Analysis and interpretation of the data: E.M, C.V., D.M. Drafting of the manuscript: E.M., C.V., D.M.

Conflict of interest

The authors declare no competing financial interests.

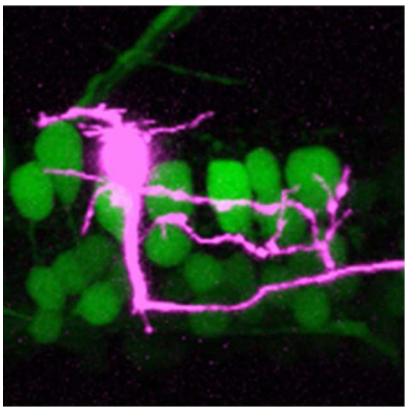

Using live imaging and labeling approaches, the authors demonstrate that a major population of spinal premotor excitatory interneuron, the V2a cells, exhibits systematic variations in morphology and synapse distribution related to their recruitment order during swimming in larval zebrafish.

Keywords

spinal cord; premotor interneurons; locomotion; *Danio rerio*

Introduction

Neural circuits are defined by their cellular components and synaptic connections. For spinal locomotor circuitry, glutamatergic interneurons with ipsilateral excitatory synapses are a phylogenetically conserved motif (Grillner and Jessell, 2009; Kiehn, 2011; Roberts et al., 2010; Stein, 2010). In fishes, frogs and mammals, the neurons that likely fulfill this role are called V2a neurons, which arise from the p2 progenitor domain and are marked by the transcription factor Chx10 (Arber, 2012; Goulding, 2009). Recent work in mice has revealed significant heterogeneity in morphology, electrical properties, connectivity and reliability of recruitment among lumbar V2a neurons regulating limb movements (Crone et al., 2008; Dougherty and Kiehn, 2010; Zhong et al., 2010; Zhong et al., 2011; Zhong et al., 2012). Consequently, it is unclear whether a uniform spinal wiring diagram can explain limb-based locomotion over the full range of speeds.

In zebrafish larvae, as in mice, V2a cells provide rhythmic locomotor drive to motoneurons (Eklof-Ljunggren et al., 2012; Kimura et al., 2006). As larvae swim faster, motoneurons are recruited according to their size, from small ventrally located motoneurons to larger dorsal ones, such that at the fastest speeds almost the entire pool is activated (McLean et al., 2008; Menelaou and McLean, 2012). While spinal V2a cells are also recruited from ventral to dorsal (McLean et al., 2007), the ventral cells active at lower swim frequencies are inhibited as frequency increases and more dorsal ones are engaged (McLean et al., 2008). To account for the pattern of axial motoneuron recruitment, dorsally located V2a cells presumably exert greater influence over the axial motor pool than more ventral V2a cells. Given the matching topographic patterns of recruitment, this relationship should be reflected by systematic

differences in V2a cell projection patterns. If such differences in morphology, and thus connectivity, related to speed do exist, this would represent an important, yet unappreciated parameter in axial locomotor networks (Borisyuk et al., 2011; Kozlov et al., 2009).

Here, we characterize the morphology and synapse distribution of spinal V2a cells to examine potential connectivity patterns within the spinal network. Unlike hindbrain V2a cells (Kimura et al., 2013; Kinkhabwala et al., 2011), morphological information related to differences in function is scarce for spinal V2a neurons. V2a cells originally termed circumferential descending (CiD) interneurons are bifurcating, with major ascending and descending axons (Bernhardt et al., 1990; Hale et al., 2001; Kuwada et al., 1990). There are also V2a cells that have an exclusively descending axon with extensive proximal collaterals, called “dorsally displaced” cells (Kimura et al., 2006; McLean et al., 2008). However, variability in axon projection patterns related to recruitment order, and thus putative connections to the axial motor pool, is unknown. Using single cell *in vivo* labeling approaches, we demonstrate that spinal V2a neurons are not homogeneous, but rather exhibit systematic differences in projection patterns and synapse distribution related to dorso-ventral position and recruitment order. Our results motivate spinal wiring diagrams for axial networks that include more variable V2a components and connections to explain movements of varying speeds.

Materials and methods

Fish

Adult wild-type and transgenic zebrafish were maintained at 28.5°C on a 14/10-h light/dark schedule in a custom built facility (Aquatic Habitats). Transgenic fish lines included Tg[chx10:GFP], Tg[chx10:Kaede] and Tg[chx10:loxPDsRed-GFP] (Kimura et al., 2006). Chx10 is a transcription factor that selectively labels V2a neurons and was formerly known as Alx (Kimura et al., 2006; Kimura et al., 2013). We also used the enhancer trap line *parg*^{mn2Et} to identify axial motoneurons (Balciunas et al., 2004). Zebrafish embryos were obtained from daily crosses of adults and raised at 28.5°C. All experiments were performed at room temperature (~22-25°C) using free-swimming 4-5 day old larval zebrafish. At this developmental stage zebrafish have not yet sexually differentiated and are still nourished by their yolk. All procedures described below conform to NIH guidelines regarding animal experimentation and were approved by the Northwestern University Institutional Animal Care and Use Committee.

DNA constructs and microinjection

We used the Gal4-UAS system to drive stochastic expression of reporter constructs selectively in V2a neurons (Koster and Fraser, 2001). Gal4 was driven by the zebrafish Chx10 gene (chx10:Gal4; Kinkhabwala et al., 2011). Reporter constructs containing upstream activating sequences (UAS) included the membrane associated fluorescent proteins mCD8:GFP and mCherry-CAAX (gifts from Dr. Joseph Fetcho, Cornell University, Ithaca, NY), cytosolic fluorescent protein tdTomato (Ben Fredj et al., 2010), and synapse specific fluorescent proteins Syp:GFP (Meyer and Smith, 2006), Syp:GCaMP3 (Nikolaou et al., 2012) and PSD95:GFP (Niell et al., 2004). Also, we generated a UAS:pTagRFP

construct from pTagRFP-N (Evrogen) with the Tol2kit (Kwan et al., 2007). Using PCR-amplification, the pTagRFP insert was flanked by gateway cloning sites (5' GGGGACAAGTTTGTACAAAAAAGCAGGCTTAACCATGGTGTCTAAGGGCGAA; 3' GGGGACCACTTTGTACAAGAAAGCTGGGTATCAATTAAGTTTGTGCCC), subcloned into a middle entry vector, and further subcloned to be under the control of a 10x element UAS promoter. Stochastic V2a expression was obtained by co-injecting the chx10:Gal4 plasmid with different combinations of the reporter constructs into one- to four-cell stage wild-type or *parg*^{mn2Et} embryos using a microinjector (Model IM300, Narishige). DNA solutions were prepared at concentrations between 15-25 ng/μl.

Kaede photoconversions

Tg[chx10:Kaede] larval zebrafish were first anesthetized in 0.02% w/v MS-222 (ethyl 3-amino- benzoate methanesulfonic acid; Sigma-Aldrich), placed in a glass bottomed dish, and embedded on their side in low-melting-point agar (1% in system water). Once the agar solidified, more anesthetic solution was added to prevent agar desiccation and movement of the fish. To visualize and photoconvert the Kaede protein, we used an Ultima two-photon laser-scanning microscope (Prairie Technologies) equipped with an ultrafast pulsed laser (Chameleon Ultra II, Coherent), a supplementary 405 nm laser line, and a 40×/1.0 numerical aperture (NA) water-immersion objective (Zeiss). Laser wavelengths of 880 and 920 nm were used to visualize the unconverted green and converted red Kaede protein, respectively. Mulitphoton images were acquired using Prairie View (Prairie Technologies). The 405 nm laser was fiber-optically coupled to Prairie Ultima scan head and was controlled using WinFluor software (Dempster et al., 2002). To prevent photo-damage in highly pigmented areas, a high magnification field of view limited to the spinal cord was first identified using bright field illumination and then the appropriate focal plane was found using laser-scanning Dodt contrast imaging. From this point, laser scanning was set to a single focal plane in the middle of Kaede-expressing somata. The duration of the each photoconversion trial was 500 milliseconds, with the laser power set to 10mW. The number of photoconversions was empirically determined for each cell (ranged between 3-10) by visually confirming the amount of red Kaede fluorescence in the soma between trials. Following the photoconversion protocol, larvae were removed from agar and were allowed to recover for 2-4 hours in a light-tight container at 28.5°C. This amount of time is more than sufficient to allow diffusion of the converted red Kaede protein from the soma to the most distal neuronal processes.

Single cell electroporations

Tg[chx10:GFP] larvae and double transgenic larvae generated by crossing the Tg[chx10:loxPDsRed-GFP] and *parg*^{mn2Et} lines were first anesthetized and then pinned right side down through the notochord using electrolytically sharpened tungsten pins to a Sylgard lined glass-bottomed dish containing 0.02% w/v MS-222 in extracellular solution (composition in mmol/l: 134 NaCl, 2.9 KCl, 1.2 MgCl2, 2.1 CaCl2, 10 HEPES, 10 glucose, adjusted to pH 7.8 with NaOH). A single spinal segment was exposed for cellular targeting by first removing the skin using fine forceps and carefully dissecting away muscle fibers using a sharpened tungsten dissecting pin. Electrodes with 0.5-1 um tip diameters were made from standard-wall 1 mm outer diameter borosilicate capillaries (A-M Systems) using

a micropipette puller (Flaming/Brown; Sutter Instrument). Pipettes were filled with AlexaFluor 647 (10,000 molecular weight, Molecular Probes, Life Technologies) diluted in patch solution (composition in mmol/l: 125 K-gluconate, 2.5 MgCl2, 10 EGTA, 10 HEPES, 4 Na2ATP, adjusted to pH 7.3 with KOH). Dye-filled pipettes were then advanced into spinal cord using a motorized micromanipulator (Sutter Instruments) until the tip was in direct contact with V2a somata, as determined by the expression of fluorescent protein. Targeting was additionally confirmed using differential interference contrast optics. A brief series of electrical stimuli were then applied (1.5-3.5V, 500ms train of 1-ms duration pulses at 100Hz). Successful electroporations were evaluated by briefly switching to an epifluorescent light source. Larvae were set aside for 30 minutes to allow for the transport of dye throughout the neuron before imaging.

In vivo imaging and morphological analysis

Zebrafish larvae were anesthetized and embedded in agar (1.4% in system water), as described above. Images were acquired using a confocal microscope (Zeiss LSM 710) equipped with an Argon laser (488 nm) and a Helium/Neon laser (543 nm) using a Zeiss 40×/1.0 NA or a 20×/1.0 NA water immersion objective. For any given V2a neuron, multiple z-stacks were acquired to capture the entire morphology of the cell. Step size for z-stacks ranged between 0.7-1 μm. Multiple confocal image stacks from a single V2a neuron were first combined together using XuvTools stitching software (Emmenlauer et al., 2009). The “stitched” files were then exported and cell morphologies were reconstructed into a three-dimensional image using Imaris software (Bitplane). Axon length measures of each reconstructed V2a neuron were obtained from Imaris. Detection of putative boutons was performed using the “Spot” function in Imaris with a spot diameter set at 0.875 μm (semi-automatic detection). Since fluorescence signals of Syp:GFP varied from cell-to-cell, we used spot detection filters within Imaris that accounted for signal differences. Accurate identification of punctate bouton labeling following filtering was always confirmed by eye.

Dorso-ventral soma positions were measured from the center of the cell body and normalized to a measurement of the dorsal and ventral edges of the spinal cord using ImageJ. The dorso-ventral location of axon filament and putative synaptic boutons within spinal cord was analyzed using a custom written MATLAB script interfaced with Imaris. Briefly, the dorsal and ventral boundaries of spinal cord were identified and then subdivided into ten equally distributed dorso-ventral bins normalized from 0 (ventral edge of spinal cord) to 1 (dorsal edge). The presence of axon filament and the number of boutons within a given division/bin was then calculated. The minimum and maximum dorso-ventral bin at which axon filament was present was used to obtain dorso-ventral axon span information with respect to soma position. For proximal and distal analysis, the rostral edge of the soma was set to 0 μm and then axon and synaptic bouton measurements were taken in 100 μm increments. Measures of bouton density were calculated as the number of boutons divided by the axon length in 100 μm increments. In proximal locations, measurements of bouton density were calculated from the point on the axon where the first synaptic bouton was observed. Cell counts from *parg*^{mn2Et} and Tg[chx10:GFP] larvae were performed using ImageJ. Segment boundaries were defined as the mid-point of the intermyotomal clefts with respect to the dorso-ventral edges of the spinal cord. For illustration purposes, snapshots of

morphological reconstructions were captured in Imaris. Using Adobe Photoshop images were then cropped and adjusted for brightness and contrast where necessary. All figures were prepared using Adobe Illustrator.

Functional imaging and electrophysiology

To measure activity-dependent increases in fluorescence levels using the genetically encoded calcium indicator GCaMP3 (Tian et al., 2009), we injected a combination of chx10:Gal4 and both Syp:GCaMP3 and ptagRFP into wild-type embryos. The expression of ptagRFP was used to screen for fish with successful expression because the baseline fluorescence intensity of Syp:GCaMP3 is not easily detectable to the naked eye using an epifluorescence stereomicroscope. The expression of ptagRFP also served as a useful measure of neuronal morphology, since synaptophysin labeling is highly punctate and restricted to synapses (Dreosti et al., 2009). Zebrafish larvae were first immobilized by immersion in recording solution containing the neuromuscular blocker, 0.1% w/v α-bungarotoxin (Tocris Bioscience) in extracellular solution. After 5–10 min, immobilized larvae were transferred to a Sylgard-lined glass-bottom dish and secured as described above. Next, the skin from 3-4 segments rostral to the caudal pin was carefully removed using fine forceps to expose the underlying muscle for ventral root recordings (muscle segments 19-25). Suction electrodes for recording extracellular motor nerve signals were made as described previously (Menelaou and McLean, 2012). Extracellular ventral root signals were acquired using a Multiclamp 700B amplifier, a Digidata series 1322A digitizer, and pClamp software (Molecular Devices). Motor nerve signals were recorded at a gain of 500 with low- and high- frequency cutoffs set at 100 and 4000 Hz, respectively. To evoke a motor output, a tungsten bipolar electrode was placed adjacent to the ear on the opposite side of the body as imaging and ventral root recordings using a manual micromanipulator (YOU-3; Narishige). Brief electrical stimuli (5–25 V; 0.2–1 ms) were delivered via an isolated stimulator (model 2100; A-M Systems).

Time series image acquisition was performed using confocal microscopy as described above. For each cell, 1-5 fields of view along the length of the axon were imaged for calcium responses. Exposure time (90-230 ms), pixel resolution and laser intensity were optimized to visualize fluorescence signals for each cell. Each trial consisted of a baseline period of 2-3 s before an electrical stimulus was applied to elicit motor activity (trial duration = 10 s). At least 4 trials were performed for each cell. The time between each trial was between 1-2 minutes. At the end of functional imaging, high quality images of Syp:GCaMP3 and ptagRFP labeling at 1024×1024 pixels resolution were captured. Ventral root recordings and Syp:GCaMP3 imaging were synchronized by a transistor-transistor logic (TTL) pulse generated by the initiation of laser scanning.

To analyze differences in fluorescence signals before, during and after motor activity, circular regions of interest (ROIs) covering putative synaptic boutons and interbouton areas were drawn using ImageJ. Fluorescent intensity measures for selected ROIs were processed for changes in intensity from baseline values ($\Delta F/F$) using custom written macros in Igor Pro 6.2 (WaveMetrics). The $\Delta F/F$ of each trial was calculated as $(F–F_0)/F_0$, where F_0 is the baseline fluorescence signal averaged over a 2 second baseline period immediately before

electrical stimulation. The signal-to-noise ratio (SNR) was calculated as the peak Δ*F/F* amplitude within a 500 ms window following the stimulus divided by the baseline noise one second prior to electrical stimulation for 3-5 trials. We only analyzed Syp:GCaMP3 responses during the first bout of motor activity following electrical stimulation.

Statistical analysis

Before statistical analysis, all data were tested for normality to determine whether parametric versus nonparametric examinations were appropriate. Consequently, comparisons of the means between two groups were performed using a paired two-sample T-test, multiple comparisons were performed using a one-way ANOVA, followed by a *post hoc* Tukey Honest Significant Difference test, and correlations were determined using a Spearman rank *R* correlation test. Degrees of freedom (*d.f.*) are reported with appropriate statistical values for each test according to convention. Statistical analysis was performed using StatPlus Professional (AnalystSoft) in conjunction with Microsoft Excel. Data are presented as means ± standard deviations. Significance was set at $p < 0.05$.

Results

In 4–5 day old zebrafish, V2a neurons form a continuous longitudinal column from the midbrain/hindbrain boundary to the caudal-most extent of spinal cord (Fig. 1A). Since the number of V2a cells in spinal cord is unknown, we first took advantage of the Tg[chx10:GFP] fish (formerly known as Tg[alx:GFP]; Kimura et al., 2006) to estimate the number of V2a cells per spinal segment. Along the length of spinal cord, there were about 20 cells per hemi-segment (Fig. 1B). Notably, this is about half the number of axial motoneurons per hemi-segment at mid-body (Menelaou and McLean, 2012). To characterize spinal V2a neuron morphology, we used three complementary approaches. First, stochastic labeling of individual neurons by co-injection of Gal4-UAS DNA constructs provided an easy, unbiased sampling of cells that labels the finest neuronal processes (Fig. 1C). Next, targeted photo-conversion of individual neurons expressing the ultraviolet sensitive fluorescent protein, Kaede (Ando et al., 2002), permitted acute and efficient sampling of V2a cells at any dorso-ventral location (Fig. 1D). Finally, targeted delivery of fluorescent dye using single cell electroporation reliably labeled the entire neuron, which further validated the other approaches (Fig. 1E). There were no obvious differences in the morphological features of neurons labeled using these three methods (Fig. 1C-E), so we have pooled the data ($n = 106$).

Given the known differences in V2a cells with respect to their ascending and descending axons, we first assessed the representation of cells with these features in our dataset. Consistent with previous reports in zebrafish (Bernhardt et al., 1990; Hale et al., 2001; Kimura et al., 2006; Kuwada et al., 1990), all spinal V2a cells had descending axons, a subset of which also had a major ascending axon ($n = 25$ of 106). Initial analysis revealed previously unappreciated morphological heterogeneity. For instance, the length of the ascending axon varied markedly (Fig. 2A–D). For some V2a neurons a long ascending axon was observed, which could project into the hindbrain, as far as rhombomere 1 (Fig. 2A, B) or remain within the spinal cord (Fig. 2C). In other V2a cells, the ascending axon projected

only a few body segments (Fig. 2D). There were also examples of V2a cells with only descending axons (Fig. 2E, F), among which some exhibited extensive local branching while others exhibited very little. In contrast to this heterogeneity, several consistent features were found in the V2a population. For example, in V2a cells with long or short ascending axons, the point of bifurcation was found at a stereotyped location on the main descending axon (Fig. 2G). In purely descending V2a cells, this same location was usually associated with local collateral elaboration (Fig. 2G).

Based on these observations, we divided the V2a population into two groups; V2a-B (bifurcating) cells with ascending projections that extended greater than 1 segment beyond the spinal segment containing the soma and V2a-D (descending) cells with either no ascending projections or ones that projected less than 1 segment rostrally. We chose 1 body segment as a conservative cut-off to differentiate V2a cells with a major ascending branch from ones with elaborate proximal collaterals that could extend into the neighboring segment. Figure 2H illustrates the axon projection distances of all of the V2a cells subdivided into V2a-B and V2a-D classes. The axon lengths vary considerably, especially among the V2a-D class, whose descending projections ranged from 1 up to 20 body segments. There was no obvious relationship between projection distance and rostro-caudal location; V2a-D neurons with short descending axons or V2a-B neurons with short ascending axons were just as likely rostrally as they were caudally. The only rostro-caudal relationship in our dataset was that the relative proportion of V2a-B cells progressively decreased from head to tail (Fig. 2I). Thus, more rostral V2a cells had the potential for ascending interactions, extending into the hindbrain, as well as descending ones within spinal cord.

Long-range and local V2a neuron innervation in relation to dorso-ventral soma position

Our observations thus far confirm that V2a cells can influence not only caudal spinal neurons (V2a-D and V2a-B) but also rostral ones (V2a-B). From the initial analysis, it appears that axon lengths vary considerably (Fig. 2I). Therefore, we first tested whether a relationship existed between dorso-ventral soma position and axon length. Figure 3A illustrates morphological reconstructions of V2a-D cells organized by their dorso-ventral soma position. This demonstrates that more dorsal V2a-D cells have systematically longer axons (Fig. 3B; Spearman's $R = 0.63$, $d.f. = 55$, $p < 0.001$, $n = 57$). In contrast, for V2a-B cells there was no significant relationship between soma position and descending axon length (Spearman's $R = –0.23$, $d.f. = 18$, $p = 0.329$, $n = 20$). Compared to V2a-D cells, the length of the descending axon was consistently long, with the majority of values falling between 1000–1500 μm (Fig. 3C). Similarly, for V2a-B cells no significant relationship was found between dorso-ventral soma position and total axon length (Spearman's $R = –0.14$, $d.f. = 18$, $p = 0.552$, $n = 20$) or between soma position and ascending axon length (Spearman's $R = –0.44$, $d.f. = 18$, $p = 0.055$, $n = 20$). Since the V2a-D and V2a-B cells were distributed over a similar dorso-ventral range (Fig. 3B,C), the lack of any significant relationship between soma position and axon length in V2a-B cells cannot be explained by differences in their distributions (e.g., V2a-B cells are all concentrated dorsally and thus longer). Thus, more dorsal V2a-D cells can potentially activate cells in more distant caudal segments

compared to more ventral V2a-D cells, while V2a-B cells have consistent rostral and caudal output regardless of dorso-ventral position.

Next, we examined differences in local V2a morphology and putative interactions with other cells related to V2a soma position. Figure 4 illustrates 5 representative examples of V2a-D (Fig. 4A) and V2a-B (Fig. 4B) cells ordered according to their dorso-ventral locations. In both V2a-D and V2a-B cells, the main descending axon projects ventrally from the soma, before turning caudally and then gradually reaching a more dorsal location. The gradual dorsal projection of the main descending axon is also obvious in lower magnification reconstructions (Fig. 2A-B, 3A). The length of the initial ventrally directed portion of axon was a function of dorso-ventral soma position; more dorsal cells had longer ventrally projecting axon segments. Also, the axon collaterals originating from the main descending axon tended to project dorsally when the main descending axon was located ventrally, and ventrally when the main axon was more dorsally located. This distinction was particularly obvious in V2a-B cells (Fig. 4B). In the majority of V2a-B cells, the trajectory of the ascending axon rose more rapidly compared to the descending axon (Fig. 4B).

To quantify putative local interactions, the dorsal-most and ventral-most location of axon was related to dorso-ventral soma position in both classes. Analysis was restricted to a proximal region 100 μm rostral and 200 μm caudal to the soma, a range that captures the gradually rising descending axon (in both classes) and the more rapidly rising ascending axon (in V2a-Bs). A consistent pattern emerges following this analysis (Fig. 4C); the vast majority of V2a cells (n = 78 of 93) extend their main axon and/or collaterals at and ventral to their own soma location. For V2a-D cells, the number and length of primary and secondary collaterals off the main axon was highly variable (Fig. 4A), and exhibited a positive significant trend between dorso-ventral position and total proximal axon length (Fig. 4D; Spearman's R = 0.43, $d.f.$ = 74, p < 0.001, n = 76). Thus, more dorsal V2a-D cells had more elaborate axons. For V2a-B neurons, the most dorsal cells had primary and secondary collaterals projecting off both the main ascending and descending axons resembling the most dorsal V2a-D cells (cf. Fig. 4A, B top) and those previously described as “dorsally displaced” (Kimura et al., 2006; McLean et al., 2008). More ventral V2a-B cells typically had a descending and ascending axon that lacked extensive proximal collaterals (Fig. 4B), reminiscent of the classic CiD-type morphology (Bernhardt et al., 1990; Hale et al., 2001; Kuwada et al., 1990). As with V2a-D cells, more dorsal V2a-B cells had longer proximal axons (Fig. 4E; Spearman's R = 0.89, $d.f.$ = 15, p < 0.001, n = 17). These findings are consistent with the idea that more dorsal V2a cells have a greater potential for activating cells throughout the dorso-ventral axis.

Using in vivo expression of synaptophysin and PSD95 to assess V2a neuron output and input

To ascertain the sites of the axon where there might be transmitter release, we used two complementary *in vivo* labeling strategies. In the first, synaptophysin coupled to GFP (Syp:GFP) was used to label sites of vesicular release (Javaherian and Cline, 2005; Li et al., 2010; Meyer and Smith, 2006). In the second, post-synaptic density protein 95 (PSD95) coupled to GFP (PSD95:GFP) was used to label sites of excitatory post-synaptic

specializations (Niell et al., 2004; Sanchez et al., 2006). Figure 5 illustrates examples of a dorsal (Fig. 5A–C) and ventral (Fig. 5D–F) V2a cell, in which co-expression of Syp:GFP and red spectrum fluorescent proteins (either mCherry or TdTomato) reveal synapse location and cellular morphology, respectively. Syp:GFP labeling was highly punctate (Fig. 5A–F), reflecting its concentration at pre-synaptic sites. This distinctive labeling made it easy to identify which sections of the axon could or could not release neurotransmitter. In Figure 5G–I is an example of co-expression of PSD95:GFP and ptagRFP (n = 11), illustrating highly punctate labeling in the small branches projecting off the initial axon segment and the initial axon segment itself. Syp:GFP was notably absent from this initial portion of the axon, particularly in more dorsal cells (Fig. 5A–F). Therefore this proximal region of axon likely serves as a site for chemical excitatory synaptic input rather than output.

Since this portion of axon would be included in our measures of axon distribution, we next compared the dorso-ventral location of proximal synaptic boutons versus axon arborization in all 26 Syp:GFP cells, as shown in Figure 5J. To compare axon and synapse location the spinal cord was divided into 10 equal bins normalized to the dorsal and ventral edges of spinal cord. There was a strong correlation between axon and synapse location. The vast majority of measurements fell along the unity line and only in a few cases were there deviations that exceeded more than one dorso-ventral bin (2 of 52), indicating that axon was present but with no synapse. This assessment validated the use of axon distribution as a reasonable metric of V2a putative output, since most putative synaptic sites were located in the same region where axon was present. To further offset any concerns about overestimating dorsal V2a neuron output based on their longer non-functional initial segments, a comparison of somatic dorso-ventral location to the density of synaptic boutons revealed that more dorsal V2a cells had higher densities per unit axon (Fig. 5K; Spearman's R = 0.64, $d.f.$ = 17, $p < 0.01$, n = 19). Although there was a similar positive trend in V2a-B cells (Fig. 5L), it was not significant (Spearman's R = 0.57, $d.f.$ = 5, p = 0.18, n = 7). The fact that more dorsal V2a cells not only have more elaborate proximal axon collaterals but also, at least for the V2a-D cells, more synapses per unit axon, is consistent with more dorsal cells having systematically higher local output.

Although the punctate nature of Syp:GFP labeling was consistent with synaptic localization, to further evaluate putative synapses, we selectively expressed Syp:GCaMP3 in V2a cells and monitored calcium transients during ‘fictive’ motor behavior (Fig. 6A). Combination of synaptophysin with a genetically encoded calcium indicator (GECI), like GCaMP, has been used by others to identify synapses (Dreosti et al., 2009; Walker et al., 2013). This is because any response from a GECI relies on calcium influx, which is largest at pre-synaptic terminals during neurotransmitter release (Koester and Sakmann, 2000). A brief electrical stimulus was applied to the head to evoke motor responses, which reliably activates V2a cells (Bhatt et al., 2007). Putative synaptic boutons were selected using the same criteria used to analyze Syp:GFP expression, since the punctate labeling of Syp:GCamP3 was indistinguishable from Syp:GFP (Fig. 6B). Interbouton locations were selected at least 1-2 μm away from putative boutons. At stimulation intensities below threshold for evoking motor activity, there was no increase in fluorescence at either bouton or interbouton locations (Fig. 6C). However, when motor activity was evoked, fluorescence intensity

increased, but only at the bouton sites (Fig. 6D). Therefore, responses at bouton sites were dependent on motor activity and not the stimulation itself. This was consistent over multiple trials and multiple boutons in the same fish (Fig. 6E). The response magnitude tended to be highest during the first swimming bout following the stimulus (Fig. 6D), when motor activity is typically most vigorous (Bhatt et al., 2007).

To assess our ability to detect supra-threshold responses at pre-synaptic locations during fictive motor behavior, we used the signal-to-noise ratio (SNR) to measure the dynamic range of the responses at boutons and interboutons in response to head stimuli (Dreosti et al., 2009). Figure 6F reveals that the majority of putative boutons had a SNR greater than 2, whereas most interboutons had a SNR less than 2. Specifically, only 6 of 257 boutons had a SNR less than 2, while 6 out of 63 interboutons had values above 2 (n = 7 fish). This clear separation is consistent with the differences in the fluorescence responses we observe at these sites (Fig. 6E). These findings suggest a functional difference in the level of calcium influx at boutons versus interboutons, with boutons exhibiting larger overall responses. Since the level of indicator is likely to play a role in detecting fluorescence responses, and levels of Syp:GCamP3 were consistently higher at punctate, bouton-like structures, care should be taken in interpreting these results. However, the observation that labeling is so highly punctate in nature and that calcium transients can be recorded at these sites argues more in favor of synapses than it does for the punctate aggregation of Syp:GCaMP3 representing non-synaptic swellings along the axon (where calcium channels are presumably less concentrated). Thus, these data lend support to our assessment of pre-synaptic distribution using Syp:GFP.

Differences in the dorso-ventral distribution of local versus long-range V2a output

Our assessment of V2 cell axon and synapse distribution revealed clear differences in their local interactions. Interestingly, as the main ascending and descending axons extended away from the soma they exhibited a gradual dorsal projection (Fig. 4A, B). To assay differences in the dorso-ventral nature of V2a output along the body axis with reference to the axial motor pool, V2a neurons were labeled in an enhancer trap line of fish (*parg*^{mn2Et}) in which motoneurons express GFP (Balciunas et al., 2004). For both V2a-D and V2a-B cells, we observed putative sites of somatic contact with motoneurons at both proximal and more caudal locations (Fig. 7A–D), as judged by the proximity of terminal collaterals and *en passant* swellings in a single optical plane (0.7–1 μm). We also observed axon collaterals and *en passant* swellings in the cell body layer that did not appear to project directly to motoneuron somata, consistent with the idea that V2a cells also make somatic connections to other spinal neurons. Unfortunately, dendritic connections were harder to assess, given the diffuse GFP labeling in the neuropil. However, since V2a axons were observed in the neuropil, *en passant* dendritic connections are more than likely to occur. Notably, at more caudal locations, the dorsal position of the main axon and collaterals corresponded to the dorsal-most extent of the axial motor pool (Fig. 7B, D). To evaluate the consistency of the dorsal projection pattern of the main axon, the ventral most location of axon for all V2a neurons located between segments 5-15 was measured at proximal (0 to 200 μm from the soma) and caudal (500 to 600 μm from the soma) locations (Fig. 7E). For V2a-B cells, the ascending axon (–100 to 0 μm) was also measured. A dorsal shift in minimum axon location

was significant for the descending axon of V2a-D cells (Paired two-sample T-test, $t = 2.03$, $d.f. = 34$, $p < 0.001$, $n = 35$) and both the descending and proximal ascending axon of V2a-B cells (One-way ANOVA with *post-hoc* Tukey Honest Significant Difference test, $F = 4.30$, $d.f. = 2,42$, $p < 0.001$, $n = 15$). Thus, for both classes putative distal interactions would be limited to the somata of dorsally located spinal neurons and any dorsally distributed dendrites originating from cells located throughout the dorso-ventral axis.

Is synaptic output at more distal locations, as evaluated by Syp:GFP expression, also biased dorsally? To answer this question we examined the dorso-ventral distribution of Syp:GFP boutons at the proximal and caudal locations (–100 to 200 and 500 to 600 μm, respectively). We first confirmed that the dorso-ventral range of Syp:GFP labeled cells covered the normal range over which V2a cells are found (Fig. 7F, G). Consistent with the measurements of axon distribution, synaptic boutons were distributed throughout the dorso-ventral axis (Fig. 7H). Critically, however, this distribution shifted dorsally at more caudal locations (Fig. 7H). To relate this to motoneuron distribution, cell counts were performed in the *parg*^{mn2Et} line. The proximal dorso-ventral distribution of V2a synaptic boutons exactly matched the range of motoneuron somata (Fig. 7H, I). At caudal locations, output was biased toward the more dorsal aspect of the motor column. These data are consistent with the idea that at more distal rostral and caudal locations, there is a potential dorsal bias in the excitatory drive provided by V2a cells.

Discussion

Our work reveals that V2a neurons are not a homogeneous morphological population. While all V2a neurons are descending, a morphologically distinct subset can also drive activity at rostral locations, including the hindbrain. These observations are consistent with anatomical features of V2a-like cells in the better characterized axial networks of lampreys and tadpoles (Buchanan and Grillner, 1987; Buchanan et al., 1989; Li et al., 2001; Li et al., 2006). What we demonstrate here, however, is that systematic variations in axon length, proximal collateralization and synapse density are related to dorso-ventral soma position and thus directly reflect recruitment order. Therefore, faster movements are generated by premotor interneurons with more potential for driving activity in spinal neurons than those responsible for slower movements. What might these targets be? In zebrafish larvae, V2a neurons make direct connections to motoneurons (Bhatt et al., 2007; Kimura et al., 2006). However, it is also likely that they contact other spinal interneurons in order to coordinate swimming movements. In lampreys and *Xenopus* tadpoles V2a-like cells are connected to motoneurons, other V2a-like cells, and commissural inhibitory interneurons (Buchanan and Grillner, 1987; Li et al., 2009; Li et al., 2004; Li et al., 2006; Parker and Grillner, 2000). Connections from V2a cells to motoneurons, other V2a neurons and commissural neurons are also likely in mice (Crone et al., 2008; Dougherty and Kiehn, 2010; Zhong et al., 2010).

At least for putative axial motoneuron connections, our observations provide a potential explanation for why there are more intense body bends that involve progressively less excitable motoneurons as swimming speed increases, which we summarize in Fig. 8. Proximally, the vast majority of V2a cells have the potential to drive activity in axial motoneurons located at the same dorso-ventral location and below. This pattern of

connectivity would explain the recruitment of motoneurons throughout the dorso-ventral axis at fast speeds when more ventral V2a cells are inhibited (McLean et al., 2008). Specifically, more dorsal V2a cells, which are active at fast speeds, have the capacity to drive the entire motor pool (Fig. 8A). Additionally, given the differences in the size and excitability of motoneurons along the dorso-ventral axis (McLean et al., 2007; Menelaou and McLean, 2012), it is noteworthy that all V2a neurons tend to project dorsally at more distal locations. This would generate an intersegmental, dorsal bias in V2a output and could potentially contribute to more excitatory drive to the dorsal axial motor column, where motoneurons are larger and less excitable (Fig. 8B). Given the substantial variability in morphology and synapse distribution related to soma position and thus recruitment order, these observations suggest that models of axial locomotor networks may need to include V2a neurons with varying probabilities of connections to explain movements at faster speeds. The findings also provide some useful predictions about the nature of V2a interactions within axial locomotor networks.

Predictions about the functional organization of connections in axial networks

One surprising finding is that extensive dorso-ventral collateralization is limited to local interactions. So, how are segmental motor pools fully engaged sequentially during fast swimming movements if not by more dorsal V2a neurons with uniform longitudinal output? It could be that dorsally located V2a axons activate dorsal motoneurons that in turn activate more ventral motoneurons via their intraspinal axon collaterals (Menelaou and McLean, 2012). Another possibility is that dorsally located V2a axons contact other dorsal V2a neurons, which would then engage the entire local motor pool. In support, not all of the terminal collateral outputs and *en passant* axon swellings of V2a cells are found near motoneuron somata. Of course, we cannot rule out potential connections to dorsally projecting dendrites of more ventral motoneurons and V2a cells.

Next, are there differences in the nature of proximal versus distal interactions between V2a cells and motoneurons? Experimental observations and modeling studies in lampreys and *Xenopus* tadpoles implicate V2a-like cells in the phasic excitation responsible for driving cycle-by-cycle rhythmicity in segmental pools of motoneurons (Grillner, 2003; Roberts et al., 2008). To reach spike threshold, motoneurons also receive a tonic source of background excitation (Di Prisco et al., 2000; Kasicki et al., 1989; Kimura et al., 2013; Soffe and Roberts, 1982; Soffe et al., 2009). In contrast to tonic excitation, phasic excitation has to be appropriately timed across and along the body. This is because fish must maintain a constant longitudinal phase lag of alternating activity to generate propulsive thrust (Grillner and Kashin, 1976). Estimates of head-tail delays during zebrafish swimming range from ~1 ms per segment at the slowest tail beat frequencies to ~100 μs at the fastest ones (Masino and Fetcho, 2005; McLean et al., 2008; Wiggin et al., 2012), which represents a constant phase lag of about 1-2% of the cycle time. Thus, if V2a cells do provide phasic on-cycle drive beyond their own body segment, the descending excitatory signal would need to propagate faster at high tail beat frequencies and slower at lower ones.

It could be there are systematic variations in axon conduction velocity related to recruitment order. Faster signals from more dorsal V2a cells would ensure shorter delays of segmental

muscle contractions. This has been predicted by computational models (Kotaleski et al., 1999), but has yet to be confirmed. Another way to set up differences in rates of signal propagation could be via differences in synaptic connections. Paired recordings between V2a cells and motoneurons have revealed both dual-component electrical and chemical excitatory post-synaptic potentials (Kimura et al., 2006) and predominantly electrical ones (Bhatt et al., 2007). However, it is not known if there are systematic differences in the relative contribution of chemical versus electrical synaptic transmission between V2a cells and motoneurons that match order of recruitment. Any of these scenarios would tie the recruitment order of premotor interneurons to matching delays in motor commands. In support, recent work ablating the dorsal-most V2a cells in zebrafish larvae not only eliminated fast swimming frequencies, but also increased the time it took for motor activity to travel along the body (Eklof-Ljunggren et al., 2012). These observations are consistent with the idea that the V2a neurons responsible for increases in swim frequency are also involved in the maintenance of appropriate phase lags.

If there are no differences in conduction velocities or synaptic connections related to recruitment order, another possibility is that all local influences are phasic and more long-range ones contribute to tonic background excitation. Although all spinal V2a neurons fire rhythmically, any significant longitudinal delay would result in excitation arriving at various phases of the swim cycle in more distal motoneurons. In lampreys and tadpoles, V2a-B-like neurons in the rostral spinal cord have ascending branches that project to other V2a-like cells and to reticulospinal neurons in the brainstem (Einum and Buchanan, 2006; Li et al., 2009; Li et al., 2006; Matsushima and Grillner, 1990). From these studies, the implied functions of ipsilateral ascending excitation include setting up a rostro-caudal gradient in excitability, sustaining rhythm generation by providing drive to more rostral V2a-like cells, synchronizing firing within the V2a pool, and providing an internal copy of spinal network activity to brainstem circuitry. Thus, excitatory drive from spinal V2a cells may not only pattern swimming activity but also determine when it happens and for how long. For the latter, V2a-B cells may be particularly important. It will be critical to test the nature of proximal versus distal V2a–V2a and V2a–motoneuron connections, in addition to assessments of axon conduction velocity, to help distinguish between the scenarios outlined above.

Potential impact on spinal rhythm generating circuitry in general

To understand spinal V2a circuitry, we have focused on 4-5 day old zebrafish larvae, where the presence of a clear dorso-ventral relationship between soma location and recruitment order can link morphological patterns to functional ones. In older zebrafish, a topographic functional relationship among V2a neurons is not as obvious (Ausborn et al., 2012). However, there is evidence for a functional arrangement of synaptic drive to axial motoneurons, whose somata maintain a topographic arrangement according to size and recruitment order (Ausborn et al., 2012; Gabriel et al., 2011). Thus, systematic differences in V2a morphology related to recruitment order described here, and the predicted differences in connectivity, may be maintained in older zebrafish, despite the potential dispersal of V2a somata during the ventro-lateral expansion of the spinal cord and the addition of new cells (Schneider and Sulner, 2006; van Raamsdonk et al., 1983). Indeed, previous work in adult

goldfish has demonstrated that V2a-like interneurons engaged during powerful escape responses also possess highly extensive proximal axonal branching (Fetcho, 1992; Fetcho and Faber, 1988). One way to test the persistence of morphological differences related to recruitment order would be to assess the birth-date of V2a cells in older fish. Previous work in zebrafish larvae has demonstrated that the orderly dorso-ventral arrangement of V2a cells according to recruitment order is due to their sequence of development; more dorsal, lateral V2a cells are older than more ventral, medial ones (Kimura et al., 2006; McLean and Fetcho, 2009). Thus order of development provides a reliable indication of recruitment order (i.e., younger V2a cells are recruited at slower speeds), which would likely persist in older fish despite somata dispersal.

While our predictions were focused on the nature of one-to-one connections, it is likely that there will also be varying degrees of convergence from V2a cells onto motoneurons. Cell counts in Tg[chx10:GFP] line and *parg*^{mn2Et} fish demonstrated corresponding differences in V2a and motoneuron number at different dorso-ventral locations. In both cases, there tends to be a ventral bias in the highest number of cells per spinal hemi-segment. Thus, one potential implication from our work, and that of others, is that there are fewer, older V2a cells with dense connectivity, and many, younger ones with sparser connectivity. In larval zebrafish, more ventral motoneurons appear to innervate smaller segmental muscle territories (Menelaou and McLean, 2012). Thus, for ventral cells, a lower interneuron to motoneuron ratio could provide finer control of segmental musculature. This is consistent with the slower, more precise movements observed during visually guided prey capture movements in larval zebrafish (Patterson et al., 2013; Trivedi and Bollmann, 2013). For faster movements, like escape maneuvers (Liu and Fetcho, 1999), the coarse control provided by higher premotor convergence to fewer, larger motoneurons may be more appropriate. This could represent a fundamental feature of motor control, namely ‘motor resolution’ determined by convergence of premotor connections to motoneurons, comparable to image resolution determined by retinal connections in the visual system (Masland, 2001). The potential to combine optogenetics and electrophysiological approaches in zebrafish should provide the means to easily test this idea.

Acknowledgements

We are grateful to members of the McLean laboratory for helpful discussions, to Martha Bagnall and Sandeep Kishore for comments on the manuscript, to Shin-ichi Higashijima, Joseph Fetcho and Martin Meyer for sharing fish lines and reagents, to David Wokosin for guidance during the photoconversion experiments, to Yujie “Richie” Sun for contributing to pilot experiments, to Sandeep Kishore for providing MATLAB analysis scripts, to Eli Cadoff for technical support, and to Matthew Chiarelli for fish care.

Grant support: This work was supported by NINDS-NIH R01 grant NS067299, the Esther A. and Joseph Klingenstein Fund, the Searle Scholars Program, and the Alfred P. Sloan Foundation. Additional support was provided by NINDS-NIH P30 grant NS054850.

Literature cited

Ando R, Hama H, Yamamoto-Hino M, Mizuno H, Miyawaki A. An optical marker based on the UV-induced green-to-red photoconversion of a fluorescent protein. Proc Natl Acad Sci U S A. 2002; 99(20):12651–12656. [PubMed: 12271129]

Arber S. Motor circuits in action: specification, connectivity, and function. Neuron. 2012; 74(6):975–989. [PubMed: 22726829]

Ausborn J, Mahmood R, El Manira A. Decoding the rules of recruitment of excitatory interneurons in the adult zebrafish locomotor network. Proc Natl Acad Sci U S A. 2012; 109(52):E3631–3639. [PubMed: 23236181]

Balciunas D, Davidson AE, Sivasubbu S, Hermanson SB, Welle Z, Ekker SC. Enhancer trapping in zebrafish using the Sleeping Beauty transposon. BMC Genomics. 2004; 5(1):62. [PubMed: 15347431]

Ben Fredj N, Hammond S, Otsuna H, Chien CB, Burrone J, Meyer MP. Synaptic activity and activity-dependent competition regulates axon arbor maturation, growth arrest, and territory in the retinotectal projection. J Neurosci. 2010; 30(32):10939–10951. [PubMed: 20702722]

Bernhardt RR, Chitnis AB, Lindamer L, Kuwada JY. Identification of spinal neurons in the embryonic and larval zebrafish. J Comp Neurol. 1990; 302(3):603–616. [PubMed: 1702120]

Bhatt DH, McLean DL, Hale ME, Fetcho JR. Grading movement strength by changes in firing intensity versus recruitment of spinal interneurons. Neuron. 2007; 53(1):91–102. [PubMed: 17196533]

Borisyuk R, Al Azad AK, Conte D, Roberts A, Soffe SR. Modeling the connectome of a simple spinal cord. Front Neuroinform. 2011; 5:20. [PubMed: 21977016]

Buchanan JT, Grillner S. Newly identified 'glutamate interneurons' and their role in locomotion in the lamprey spinal cord. Science. 1987; 236(4799):312–314. [PubMed: 3563512]

Buchanan JT, Grillner S, Cullheim S, Risling M. Identification of excitatory interneurons contributing to generation of locomotion in lamprey: structure, pharmacology, and function. J Neurophysiol. 1989; 62(1):59–69. [PubMed: 2754481]

Crone SA, Quinlan KA, Zagoraiou L, Droho S, Restrepo CE, Lundfald L, Endo T, Setlak J, Jessell TM, Kiehn O, Sharma K. Genetic ablation of V2a ipsilateral interneurons disrupts left-right locomotor coordination in mammalian spinal cord. Neuron. 2008; 60(1):70–83. [PubMed: 18940589]

Dempster J, Wokosin DL, McCloskey KD, Girkin JM, Gurney AM. WinFluor - An integrated system for the simultaneous recording of cell fluorescence images and electrophysiological signals on a single computer system. Br J Pharmacol. 2002:1–7.

Di Prisco GV, Pearlstein E, Le Ray D, Robitaille R, Dubuc R. A cellular mechanism for the transformation of a sensory input into a motor command. J Neurosci. 2000; 20(21):8169–8176. [PubMed: 11050140]

Dougherty KJ, Kiehn O. Firing and cellular properties of V2a interneurons in the rodent spinal cord. J Neurosci. 2010; 30(1):24–37. [PubMed: 20053884]

Dreosti E, Odermatt B, Dorostkar MM, Lagnado L. A genetically encoded reporter of synaptic activity in vivo. Nat Methods. 2009; 6(12):883–889. [PubMed: 19898484]

Einum JF, Buchanan JT. Spinobulbar neurons in lamprey: cellular properties and synaptic interactions. J Neurophysiol. 2006; 96(4):2042–2055. [PubMed: 16837656]

Eklof-Ljunggren E, Haupt S, Ausborn J, Dehnisch I, Uhlen P, Higashijima S, El Manira A. Origin of excitation underlying locomotion in the spinal circuit of zebrafish. Proc Natl Acad Sci U S A. 2012; 109(14):5511–5516. [PubMed: 22431619]

Fetcho JR. Excitation of motoneurons by the Mauthner axon in goldfish: complexities in a “simple” reticulospinal pathway. J Neurophysiol. 1992; 67(6):1574–1586. [PubMed: 1629765]

Fetcho JR, Faber DS. Identification of motoneurons and interneurons in the spinal network for escapes initiated by the mauthner cell in goldfish. J Neurosci. 1988; 8(11):4192–4213. [PubMed: 3183720]

Gabriel JP, Ausborn J, Ampatzis K, Mahmood R, Eklof-Ljunggren E, El Manira A. Principles governing recruitment of motoneurons during swimming in zebrafish. Nat Neurosci. 2011; 14(1): 93–99. [PubMed: 21113162]

Goulding M. Circuits controlling vertebrate locomotion: moving in a new direction. Nat Rev Neurosci. 2009; 10(7):507–518. [PubMed: 19543221]

Grillner S. The motor infrastructure: from ion channels to neuronal networks. Nat Rev Neurosci. 2003; 4(7):573–586. [PubMed: 12838332]

Grillner S, Jessell TM. Measured motion: searching for simplicity in spinal locomotor networks. Curr Opin Neurobiol. 2009; 19(6):572–586. [PubMed: 19896834]

Grillner, S.; Kashin, S. On the generation and performance of swimming in fish.. In: Hermann, RM.; Grillner, S.; Stein, PSG.; Stuart, DG., editors. Neural Control of Locomotion Advances in Behavioral Biology. Plenum; New York: 1976. p. 181-201.

Hale ME, Ritter DA, Fetcho JR. A confocal study of spinal interneurons in living larval zebrafish. J Comp Neurol. 2001; 437(1):1–16. [PubMed: 11477593]

Javaherian A, Cline HT. Coordinated motor neuron axon growth and neuromuscular synaptogenesis are promoted by CPG15 in vivo. Neuron. 2005; 45(4):505–512. [PubMed: 15721237]

Kasicki S, Grillner S, Ohta Y, Dubuc R, Brodin L. Phasic modulation of reticulospinal neurones during fictive locomotion and other types of spinal motor activity in lamprey. Brain Res. 1989; 484(1-2):203–216. [PubMed: 2713681]

Kiehn O. Development and functional organization of spinal locomotor circuits. Curr Opin Neurobiol. 2011; 21(1):100–109. [PubMed: 20889331]

Kimura Y, Okamura Y, Higashijima S. alx, a zebrafish homolog of Chx10, marks ipsilateral descending excitatory interneurons that participate in the regulation of spinal locomotor circuits. J Neurosci. 2006; 26(21):5684–5697. [PubMed: 16723525]

Kimura Y, Satou C, Fujioka S, Shoji W, Umeda K, Ishizuka T, Yawo H, Higashijima SI. Hindbrain V2a neurons in the excitation of spinal locomotor circuits during zebrafish swimming. Curr Biol. 2013; 23:843–849. [PubMed: 23623549]

Kinkhabwala A, Riley M, Koyama M, Monen J, Satou C, Kimura Y, Higashijima S, Fetcho J. A structural and functional ground plan for neurons in the hindbrain of zebrafish. Proc Natl Acad Sci U S A. 2011; 108(3):1164–1169. [PubMed: 21199947]

Koester HJ, Sakmann B. Calcium dynamics associated with action potentials in single nerve terminals of pyramidal cells in layer 2/3 of the young rat neocortex. J Physiol 529 Pt. 2000; 3:625–646.

Koster RW, Fraser SE. Tracing transgene expression in living zebrafish embryos. Dev Biol. 2001; 233(2):329–346. [PubMed: 11336499]

Kotaleski JH, Lansner A, Grillner S. Neural mechanisms potentially contributing to the intersegmental phase lag in lamprey.II. Hemisegmental oscillations produced by mutually coupled excitatory neurons. Biol Cybern. 1999; 81(4):299–315. [PubMed: 10541934]

Kozlov A, Huss M, Lansner A, Kotaleski JH, Grillner S. Simple cellular and network control principles govern complex patterns of motor behavior. Proc Natl Acad Sci U S A. 2009; 106(47): 20027–20032. [PubMed: 19901329]

Kuwada JY, Bernhardt RR, Nguyen N. Development of spinal neurons and tracts in the zebrafish embryo. J Comp Neurol. 1990; 302(3):617–628. [PubMed: 2262604]

Kwan KM, Fujimoto E, Grabher C, Mangum BD, Hardy ME, Campbell DS, Parant JM, Yost HJ, Kanki JP, Chien CB. The Tol2kit: a multisite gateway-based construction kit for Tol2 transposon transgenesis constructs. Dev Dyn. 2007; 236(11):3088–3099. [PubMed: 17937395]

Li L, Tasic B, Micheva KD, Ivanov VM, Spletter ML, Smith SJ, Luo L. Visualizing the distribution of synapses from individual neurons in the mouse brain. PLoS One. 2010; 5(7):e11503. [PubMed: 20634890]

Li WC, Perrins R, Soffe SR, Yoshida M, Walford A, Roberts A. Defining classes of spinal interneuron and their axonal projections in hatchling Xenopus laevis tadpoles. J Comp Neurol. 2001; 441(3): 248–265. [PubMed: 11745648]

Li WC, Roberts A, Soffe SR. Locomotor rhythm maintenance: electrical coupling among premotor excitatory interneurons in the brainstem and spinal cord of young Xenopus tadpoles. J Physiol. 2009; 587(Pt 8):1677–1693. [PubMed: 19221124]

Li WC, Soffe SR, Roberts A. Glutamate and acetylcholine corelease at developing synapses. Proc Natl Acad Sci U S A. 2004; 101(43):15488–15493. [PubMed: 15494439]

Li WC, Soffe SR, Wolf E, Roberts A. Persistent responses to brief stimuli: feedback excitation among brainstem neurons. J Neurosci. 2006; 26(15):4026–4035. [PubMed: 16611819]

Liu KS, Fetcho JR. Laser ablations reveal functional relationships of segmental hindbrain neurons in zebrafish. Neuron. 1999; 23(2):325–335. [PubMed: 10399938]

Masino MA, Fetcho JR. Fictive swimming motor patterns in wild type and mutant larval zebrafish. J Neurophysiol. 2005; 93(6):3177–3188. [PubMed: 15673549]

Masland RH. The fundamental plan of the retina. Nat Neurosci. 2001; 4(9):877–886. [PubMed: 11528418]

Matsushima T, Grillner S. Intersegmental co-ordination of undulatory movements--a “trailing oscillator” hypothesis. Neuroreport. 1990; 1(2):97–100. [PubMed: 2129876]

McLean DL, Fan J, Higashijima S, Hale ME, Fetcho JR. A topographic map of recruitment in spinal cord. Nature. 2007; 446(7131):71–75. [PubMed: 17330042]

McLean DL, Fetcho JR. Spinal interneurons differentiate sequentially from those driving the fastest swimming movements in larval zebrafish to those driving the slowest ones. J Neurosci. 2009; 29:13566–13577. [PubMed: 19864569]

McLean DL, Masino MA, Koh IY, Lindquist WB, Fetcho JR. Continuous shifts in the active set of spinal interneurons during changes in locomotor speed. Nat Neurosci. 2008; 11(12):1419–1429. [PubMed: 18997790]

Menelaou E, McLean DL. A gradient in endogenous rhythmicity and oscillatory drive matches recruitment order in an axial motor pool. J Neurosci. 2012; 32(32):10925–10939. [PubMed: 22875927]

Meyer MP, Smith SJ. Evidence from in vivo imaging that synaptogenesis guides the growth and branching of axonal arbors by two distinct mechanisms. J Neurosci. 2006; 26(13):3604–3614. [PubMed: 16571769]

Niell CM, Meyer MP, Smith SJ. In vivo imaging of synapse formation on a growing dendritic arbor. Nat Neurosci. 2004; 7(3):254–260. [PubMed: 14758365]

Nikolaou N, Lowe AS, Walker AS, Abbas F, Hunter PR, Thompson ID, Meyer MP. Parametric functional maps of visual inputs to the tectum. Neuron. 2012; 76(2):317–324. [PubMed: 23083735]

Parker D, Grillner S. The activity-dependent plasticity of segmental and intersegmental synaptic connections in the lamprey spinal cord. Eur J Neurosci. 2000; 12(6):2135–2146. [PubMed: 10886353]

Patterson BW, Abraham AO, Maciver MA, McLean DL. Visually guided gradation of prey capture movements in larval zebrafish. J Exp Biol. 2013 in press.

Roberts A, Li WC, Soffe SR. How neurons generate behavior in a hatchling amphibian tadpole: an outline. Front Behav Neurosci. 2010; 4:16. [PubMed: 20631854]

Roberts A, Li WC, Soffe SR, Wolf E. Origin of excitatory drive to a spinal locomotor network. Brain Res Rev. 2008; 57(1):22–28. [PubMed: 17825424]

Sanchez AL, Matthews BJ, Meynard MM, Hu B, Javed S, Cohen Cory S. BDNF increases synapse density in dendrites of developing tectal neurons in vivo. Development. 2006; 133(13):2477–2486. [PubMed: 16728478]

Schneider H, Sulner B. Innervation of dorsal and caudal fin muscles in adult zebrafish Danio rerio. J Comp Neurol. 2006; 497(5):702–716. [PubMed: 16786559]

Soffe SR, Roberts A. Tonic and phasic synaptic input to spinal cord motoneurons during fictive locomotion in frog embryos. J Neurophysiol. 1982; 48(6):127931288.

Soffe SR, Roberts A, Li WC. Defining the excitatory neurons that drive the locomotor rhythm in a simple vertebrate: insights into the origin of reticulospinal control. J Physiol. 2009; 587(Pt 20): 4829–4844. [PubMed: 19703959]

Stein PS. Alternation of agonists and antagonists during turtle hindlimb motor rhythms. Ann N Y Acad Sci. 2010; 1198:105–118. [PubMed: 20536925]

Tian L, Hires SA, Mao T, Huber D, Chiappe ME, Chalasani SH, Petreanu L, Akerboom J, McKinney SA, Schreiter ER, Bargmann CI, Jayaraman V, Svoboda K, Looger LL. Imaging neural activity in worms, flies and mice with improved GCaMP calcium indicators. Nat Methods. 2009; 6(12):875–881. [PubMed: 19898485]

Trivedi CA, Bollmann JH. Visually driven chaining of elementary swim patterns into a goal-directed motor sequence: a virtual reality study of zebrafish prey capture. Front Neural Circuits. 2013; 7:86. [PubMed: 23675322]

van Raamsdonk W, Mos W, Smit-Onel MJ, van der Laarse WJ, Fehres R. The development of the spinal motor column in relation to the myotomal muscle fibers in the zebrafish (Brachydanio

rerio). I. Posthatching development. Anat Embryol (Berl). 1983; 167(1):125–139. [PubMed: 6881540]

Walker AS, Burrone J, Meyer MP. Functional imaging in the zebrafish retinotectal system using RGECO. Front Neural Circuits. 2013; 7:34. [PubMed: 23508811]

Wiggin TD, Anderson TM, Eian J, Peck JH, Masino MA. Episodic swimming in the larval zebrafish is generated by a spatially distributed spinal network with modular functional organization. J Neurophysiol. 2012; 108(3):925–934. [PubMed: 22572943]

Zhong G, Droho S, Crone SA, Dietz S, Kwan AC, Webb WW, Sharma K, Harris-Warrick RM. Electrophysiological characterization of V2a interneurons and their locomotor-related activity in the neonatal mouse spinal cord. J Neurosci. 2010; 30(1):170–182. [PubMed: 20053899]

Zhong G, Sharma K, Harris-Warrick RM. Frequency-dependent recruitment of V2a interneurons during fictive locomotion in the mouse spinal cord. Nat Commun. 2011; 2:274. [PubMed: 21505430]

Zhong G, Shevtsova NA, Rybak IA, Harris-Warrick RM. Neuronal activity in the isolated mouse spinal cord during spontaneous deletions in fictive locomotion: insights into locomotor central pattern generator organization. J Physiol. 2012; 590(Pt 19):4735–4759. [PubMed: 22869012]

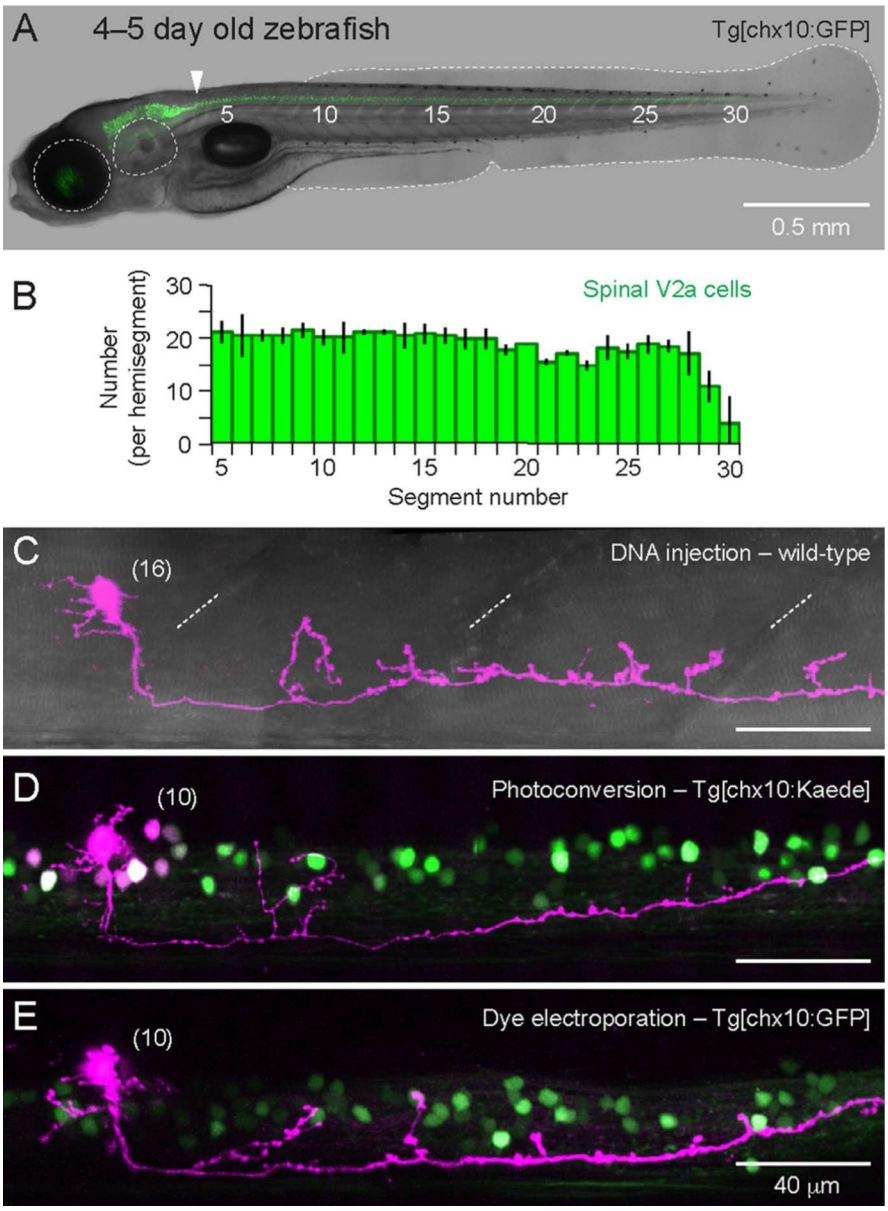

Figure 1. Labeling V2a neurons in the spinal cord

(A) Transgenic larval zebrafish in which V2a neurons are labeled with green fluorescent protein, Tg[chx10:GFP]. Muscle segments are numbered. From left to right, the eye, ear, and tail fin are outlined in white dashed lines. In this, and subsequent images, rostral is to the left and dorsal is up. A white arrowhead indicates the hindbrain–spinal cord boundary at muscle segments 3–4 (Kimura et al., 2013). Muscle segment 1 begins just behind the ear.

(B) Number of V2a cells per spinal hemisegment in the Tg[chx10:GFP] line between muscle segments 5–30. Means and standard deviations are plotted from counts in 3 different fish. There are about 20 V2a cells per hemisegment and the number decreases beyond segment 29.

(C) *In vivo* confocal z-stack image of a V2a neuron labeled with mCherry (purple) using microinjection of Gal4-UAS constructs in a wild-type embryo (DNA injection). The neuron

is superimposed on a DIC image, which reveals the segmented musculature (diagonal dashed white lines). Here and below, the body segment number is in parentheses next to the cell body.

(D) Confocal z-stack of a V2a neuron labeled by ultraviolet light photoconversion (purple) in the Tg[chx10:Kaede] line. In the background are green V2a neurons that were not photoconverted. Faintly labeled somata with varying levels of photoconverted protein (purple and white cells) in close proximity to the targeted cell are also obvious. For reconstruction purposes, the targeted cell was always the brightest one and its processes were easily traced using our three-dimensional rendering software.

(E) As in *D*, but this cell was targeted in the Tg[chx10:GFP] line and filled with Alexa-647 dextran (purple) using single cell electroporation. Note that here and in panel *D*, the somata of the targeted, most brightly labeled, cells appear larger due to the increase in gain required to reveal the finer processes.

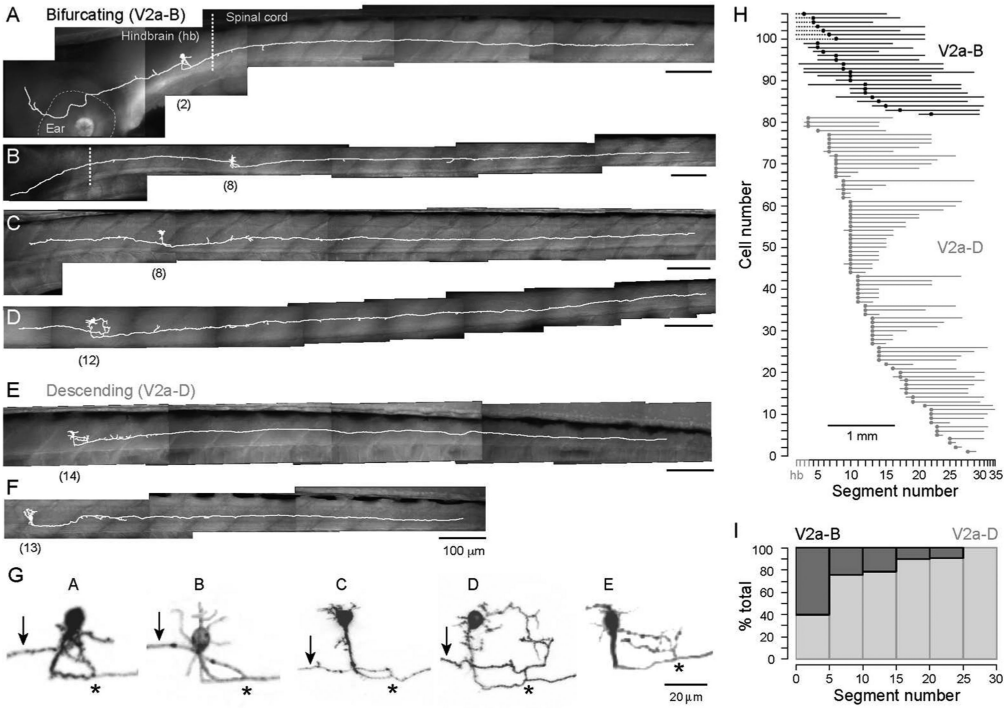

Figure 2. V2a neurons can be divided into two broad classes

(A–D) Morphological reconstructions of bifurcating V2a neurons (V2a-B) with a prominent ascending axon. V2a-B cells were defined as anything that projects more than 1 segment rostral to the spinal segment containing the soma. Reconstructions in white are superimposed on DIC images. Segment numbers are noted parenthetically below each cell. More rostrally located V2a-Bs can project well into the hindbrain (hb).

(E–F) As in *A–D*, but two examples of descending V2a neurons (V2a-D). These cells lack a prominent ascending axon.

(G) Contrast inverted confocal images of the proximal region around the somata for the images in *A–E*. An asterisk marks the origin of the ascending axon (arrow) off the main descending axon (*A–D*). For descending cells, this location is often associated with a region of local collateral elaboration (*E*).

(H) Ball and stick plots of the somata location and the axon projection distance for V2a-B and V2a-D cells (n = 106). Dashed lines in the V2a-B cells indicate ascending axons that project into the hindbrain (hb). The X-axis has been scaled to reflect the width of each body segment in 4-5 day old larvae (scale bar inset). V2a-D cells vary considerably in their projection distances, compared to V2a-B cells.

(I) Rostrocaudal distribution of the different classes as a proportion of the total number of cells at each segment. The proportion of V2a-Bs sampled decreases caudally.

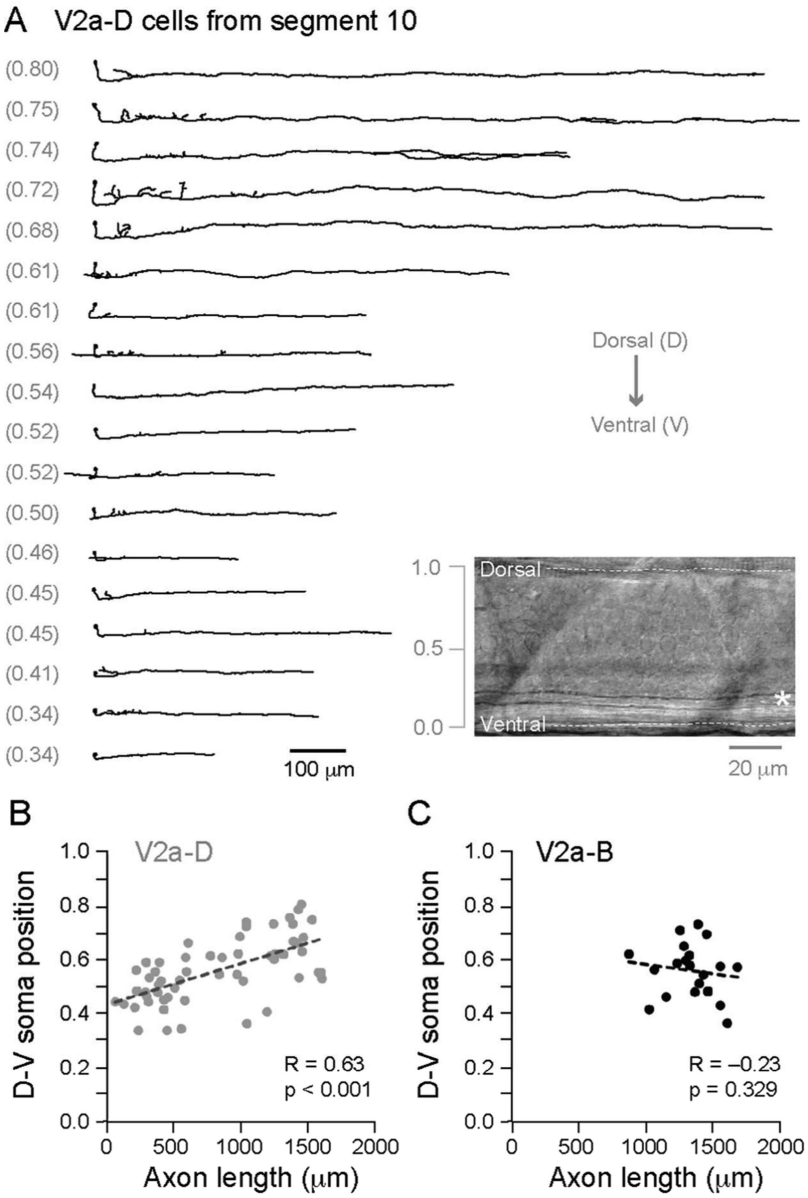

Figure 3. V2a-Ds have longer axons related to dorso-ventral soma position

(A) Reconstructions of V2a-D cells arranged from top to bottom according to their dorso-ventral location (noted parenthetically to the left). All of the cells originate from body segment 10. Inset is a DIC image that illustrates how dorso-ventral location is normalized according to the top (1.0) and bottom (0.0) edges of spinal cord. Asterisk marks the large Mauthner axon.

(B) A comparison of dorso-ventral (D-V) soma position versus descending axon length reveals a significant relationship for V2a-Ds located between segments 5-15 (n = 57). Note, we limited our analysis to this region because V2a-Ds can extend up to 20 body segments (see Fig. 2D) and we did not want the end of the spinal cord (~segment 35) to act as a limiting factor.

(C) As in *B*, but no significant relationship is found for V2a-Bs (n = 20).

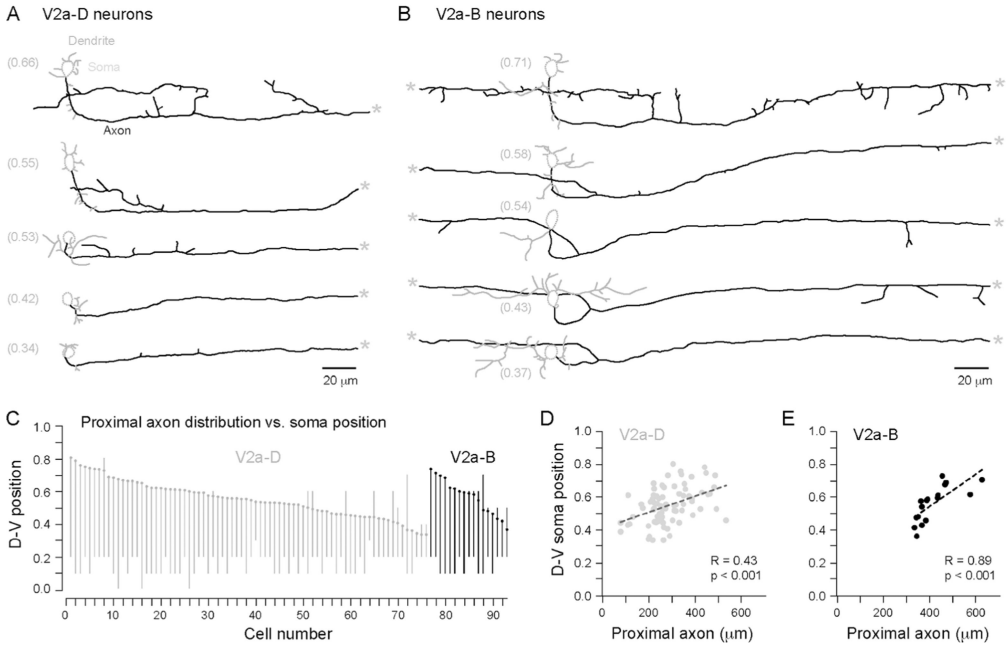

Figure 4. Proximal arborization length is related to somatic dorso-ventral location

(A) Reconstructions of V2a-D cells arranged from top to bottom according to their dorso-ventral location (noted parenthetically to the left). The main axons and collaterals (black), presumed dendrites (grey) and somata (dotted grey line) are indicated. Dendrites were defined according to criteria specified in (Li et al., 2001). A grey asterisk marks where the main axon exits the field of view.

(B) As in *A*, but for V2a-B cells.

(C) Ball and stick plots illustrating dorso-ventral (D-V) soma position and the distribution of local axon arborization for both classes (n = 93). Cells for which we could not obtain accurate measures of D-V axon position are not included (e.g., at the transition to the hindbrain, rostral to segment 5). The lines represent the maximum and minimum D-V position at which any part of the axon was observed, up to 100 μm rostral and 200 μm caudal from the soma. V2a cells tend to innervate areas at and below their somatic dorso-ventral position.

(D) A comparison of D-V soma position versus proximal axon length reveals a significant relationship for V2a-Ds (n = 76).

(E) As in *D*, but for V2a-Bs (n = 17).

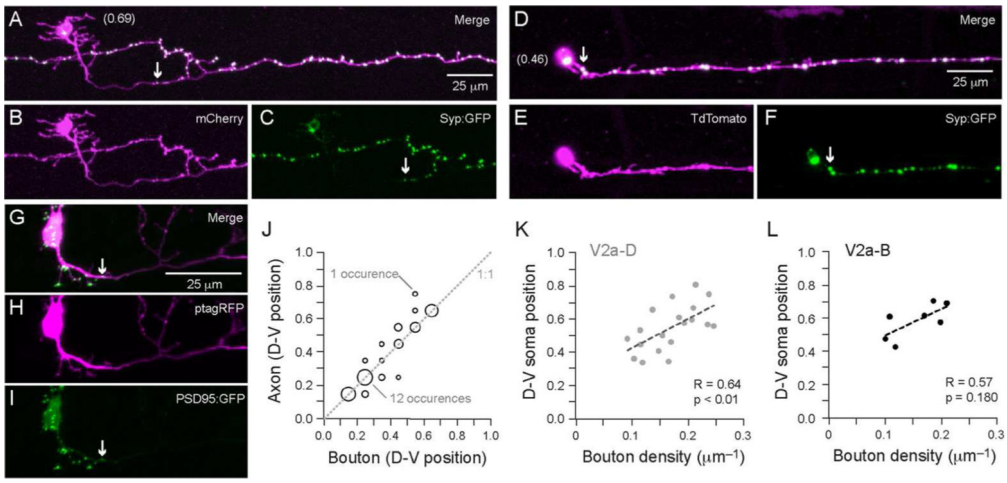

Figure 5. Localization of putative pre-synaptic sites corroborates anatomical measures

(A–C) Confocal z-stacks of co-expression of mCherry (*B*) and synaptophysin-GFP (Syp:GFP; *C*) in the same cell and the merged image (*A*). Syp:GFP labels punctate bouton-like structures, as you would expect with synapse specific targeting. A white arrow marks the first synaptic bouton. Dorso-ventral soma position is in parentheses here and in *D*.

(D–F) As in *A–C*, but a more ventral V2a cell labeled with TdTomato.

(G–I) As in *A–F*, except the post-synaptic marker PSD95:GFP (*I*) is co-expressed with ptagRFP *(H)*. Note that there is background cytosolic expression of PSD95:GFP in the soma, which is distinguishable from the punctate labeling in the dendrites, soma and axon. Again, the punctate labeling is consistent with synaptic targeting. Putative post-synaptic inputs are found on the axon up to the point at which synaptic output begins (as assessed using Syp:GFP, above). A white arrow marks the last post-synaptic density.

(J) In cells co-expressing red shifted fluorescent proteins and Syp:GFP, a comparison of the maximum and minimum D-V positions at which axon versus synaptic boutons were observed reveals a good correlation (unity line, 1:1). The plot includes two measures (maximum and minimum) per cell (n = 52 from 26 cells) from axon 100 rostral/200 μm caudal to their somata. The size of the circle represents the number of occurrences (e.g., for minimum distributions, matching axon and bouton observations between 0.1–0.2 occurred 12 times; for maximum distributions, the mismatched presence of axon between 0.7–0.8, but boutons between 0.5–0.6, occurred only once). The distribution of axon serves as a reliable reporter of functional output.

(K) A comparison of D-V soma position versus synaptic bouton density for V2a-D cells (n = 19), measured proximally (defined as 100 μm rostral and 200 μm caudal to the soma). More dorsal cells have more synapses per unit axon.

(L) As in *K*, but for V2a-B cells (n = 7). A similar trend is obvious, but is not statistically significant.

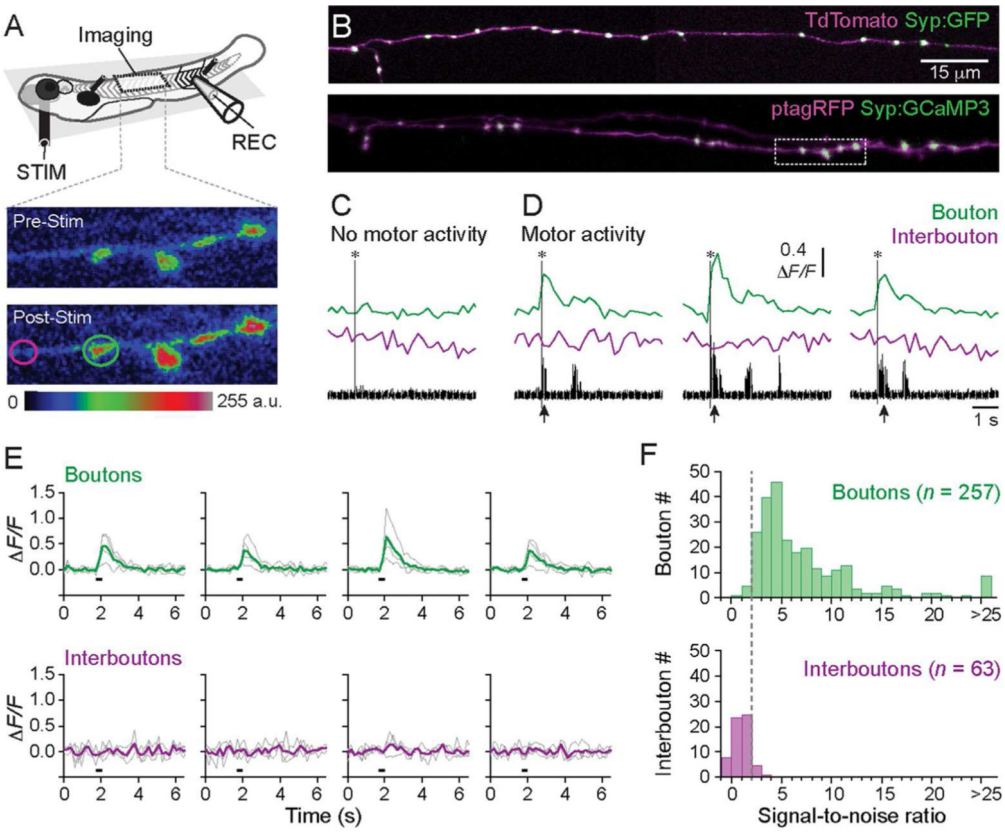

Figure 6. *In vivo* assessment of putative synaptic sites using Syp:GCaMP3

(A) Schematic of the *in vivo* preparation for simultaneous Syp:GCaMP3 imaging and motor nerve recordings in larval zebrafish. Inset shows the localized fluorescence intensity in putative pre-synaptic boutons two frames before (Pre-stim, top) and after (Post-stim, bottom) electrical stimulation. Fluorescence intensity changes are pseudo-colored in arbitrary units (a.u.).

(B) Confocal z-stacks from a V2a cell axon co-expressing TdTomato and Syp:GFP (top) and ptagRFP and Syp:GCaMP3 (bottom). Dashed box marks the regions shown inset in *A*. (C–D) Syp:GCaMP3 responses from a putative individual bouton (green) and interbouton region (purple) as indicated in the color-coded circles inset in *A*. Bouton and interbouton ΔF/F signals are illustrated following an electrical stimulation that produced either no motor activity (*C*, one trial shown) or robust motor activity (*D*, three individual trials shown), as indicated below by the rectified motor nerve recordings. Arrows indicate motor activity following stimulation. Asterisks mark the stimulation artifact.

(E) Syp:GCaMP3 responses from four boutons and four interboutons from the cell shown in *B*, bottom. Grey lines indicate the ΔF/F responses from 4 individual trials (grey lines) and the average responses across trials (bold colored lines) for boutons and interboutons. Black lines below the traces indicate the onset of the stimulation.

(F) Signal-to-noise ratio (SNR) measured at bouton and interbouton locations from 7 fish. SNR was measured as the peak amplitude of the average response immediately following the stimulus divided by the standard deviation of the baseline signal (See Materials and

Methods for details). A SNR above 2 (marked by the dashed grey line) is reliably observed at boutons.

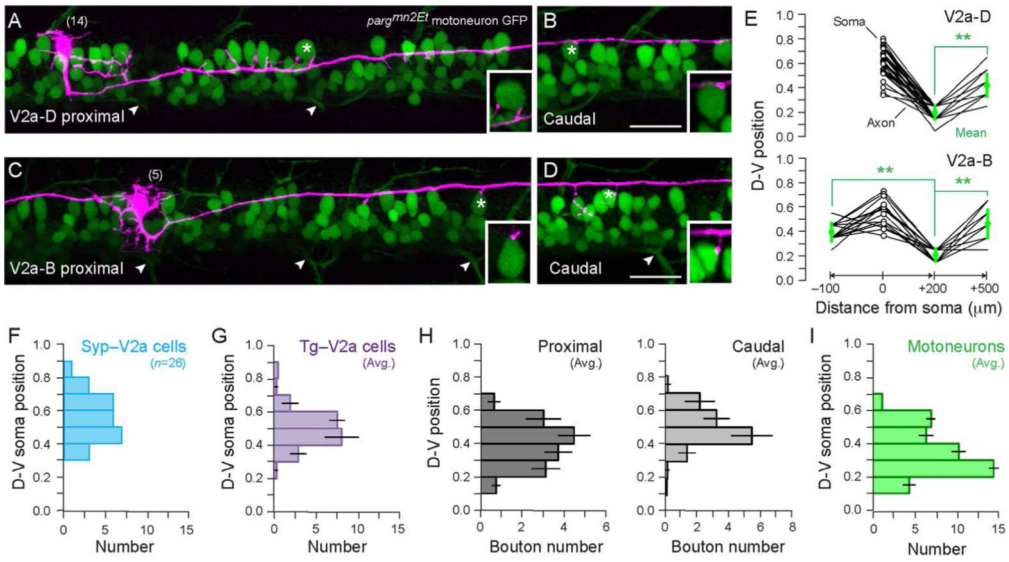

Figure 7. Long-range axon trajectories generate a dorsal bias in V2a output

(A–B) Confocal z-stack of a V2a neuron labeled with ptagRFP (purple) in a motoneuron-GFP transgenic fish (*parg*^{mn2Et}) (n=21). This is the same cell originally presented in Fig. 2E. Images are from a proximal (*A*) and a distal location ~400 μm caudal to the soma (*B*). Proximal collaterals terminate in close proximity to motoneuron somata. The distal axon follows a trajectory that indicates contact with more dorsal motoneurons and dendritic processes. Insets are from a single focal plane (0.7 μm) to demonstrate close proximity contacts to motoneuron somata marked by asterisks. Segment number is in parentheses. Arrowheads indicate ventral root exit points.

(C–D) As in *A–B* but for a V2a-B cell (n=5).

(E) Measurements of minimum axon distribution at two proximal locations (–100 to 0 μm from the soma and 0 to 200 μm from the soma) and a more caudal location (500 to 600 μm). Note the ascending measure was only performed for V2a-B cells. Minimum axon distributions are binned at 0.1 intervals normalized to the top and bottom of spinal cord. Soma values (open circles) are non-binned normalized locations. We only included cells between segments 5–15 that projected at least 500 μm (V2a-D, $n = 35$; V2a-B, $n = 15$). Means of minimum axon distributions are in green, plus and minus standard deviations. **, $p < 0.001$. There is a clear dorsal bias in minimum axon distribution at more distant locations.

(F) Dorso-ventral (D-V) distribution of all the V2a cells sampled that expressed Syp:GFP (Syp-V2a). The distribution overlaps with the real distribution of V2a cells (*G*).

(G) D-V distribution of the average number of V2a cells per hemisegment at mid-body (means and standard deviations from 3 consecutive hemisegments in 3 different Tg[chx10:GFP] larvae). V2a cells are distributed more dorsally compared to motoneurons (*I*), with the largest number found between normalized D-V positions of 0.4–0.6.

(H) Average (plus/minus standard deviations) number of synaptic boutons per normalized D-V bin for proximal (left) and caudal (right) locations (as defined above in *E*). Averages were calculated per 100 μm, as this represents the approximate width of a single muscle

segment. Proximal distributions overlap with motoneuron distributions (*I*). In caudal locations, the peak bin is still 0.4–0.5, however the distribution is shifted dorsally. (I) As in *G*, but for motoneurons. Cell counts were performed at midbody in the *parg*^{mn2Et} enhancer trap line (n = 3 consecutive hemisegments in 3 different larvae). Above the normalized D-V position of 0.2, motoneuron numbers tend to decrease dorsally.

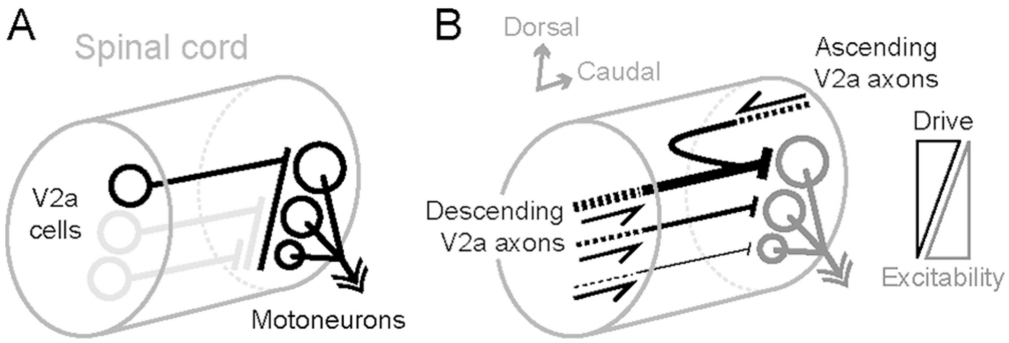

Figure 8. Proposed local and long-range interactions between V2a neurons and motoneurons. Schematic representation of V2a cells and motoneurons within spinal cord summarizes our findings with respect to their recruitment patterns during swimming

(A) Differences in local axon innervation of V2a cells demonstrate that the most dorsal V2a cells (in black) have a higher likelihood of making connections to motoneurons throughout the dorso-ventral (D-V) axis than more ventral ones (in grey), which could explain the activation of the entire motor pool during fast swimming when only more dorsal V2a cells are active.

(B) The variability in local interactions combined with the dorsal bias in long-range interactions set up a D-V gradient in V2a excitatory drive that matches motoneuron excitability.